Engineering bio-inspired peptide-polyurea hybrids with thermo-responsive shape memory behaviour

Design, System, Application Statement

Engineering bio-inspired peptide-polyurea hybrids with thermoresponsive shape memory behaviour

Daseul Jang[a‡], Chase B. Thompson[a‡], Sourav Chatterjee, [a] and LaShanda T.J. Korley [a,b]*

Nature provides an expansive toolset for the engineering of responsive materials, including the hierarchical assembly of building blocks. We are inspired by the structural arrangement in natural systems, such as spider silk, to design hybrid materials that incorporate thermoresponsive self-assembly motifs in a conventional polymeric framework. Specifically, the modulation of peptide secondary structure and hierarchical organization was utilized as handles to tailor the shape memory response in polyureas derived from peptidic copolymer soft segments. Here, the relative ratio of α-helix:β-sheet structures was controlled by varying the peptide length and composition, leading to polyurea hybrids with tunable hydrogen bonding arrangements (inter- vs. intra-molecular). Using this design approach, shape fixity and recovery are tuned due to modulation of chain elasticity, domain stability, and phase organization. These peptide assemblies also provide an additional pathway toward responsive behaviour via annealing of the secondary structure, demonstrating switchability. Our engineering strategy offers rules for developing stimuli-responsive materials via a balance of hydrogen bonding structure, morphological organization, and mechanical response to impact applications ranging from biomedical devices to electronic systems.

Engineering bio-inspired peptide-polyurea hybrids with thermo-responsive shape memory behaviour

Daseul Jang[a‡], Chase B. Thompson[a‡], Sourav Chatterjee, [a] and LaShanda T.J. Korley [a,b]*

Inspired by Nature's tunability driven by the modulation of structural organization, we utilize peptide motifs as an approach to tailor not only hierarchical structure, but also thermo-responsive shape memory properties of conventional polymeric materials. Specifically, poly(β-benzyl-L-aspartate)-b-poly(dimethylsiloxane)-b-poly(β-benzyl-L-aspartate) was incorporated as the soft segment in peptide-polyurea hybrids to manipulate hierarchical ordering through peptide secondary structure and a balance of inter- and intra-molecular hydrogen bonding. Employing these bioinspired peptidic polyureas, we investigated the influence of secondary structure on microphase-separated morphology, and shape fixity and recovery via attenuated total reflectance-Fourier transform infrared spectroscopy (ATR-FTIR), small-angle X-ray scattering (SAXS) and dynamic mechanical analysis (DMA). The β-sheet motifs promoted phase mixing through extensive inter-molecular hydrogen bonding between the hard block and peptide segments and provided an increased chain elasticity, resulting in decreased shape fixity compared to a non-peptidic control. In contrast, intra-molecular hydrogen bonding driven by the α-helical arrangements yielded a microphase-separated and hierarchically ordered morphology, leading to an increase in the shape fixing ratio. These results indicate that peptide secondary structure provides a convenient handle for tuning shape memory properties by regulating hydrogen bonding with the surrounding polyurea hard segment, wherein extent of hydrogen bonding and phase mixing between the peptidic block and hard segment dictate the resulting shape memory behaviour. Furthermore, the ability to shift secondary structure as a function of temperature was also demonstrated as a pathway to influence shape memory response. This research highlights that peptide secondary conformation influences the hierarchical ordering and modulates the shape memory response of peptide-polymer hybrids. We anticipate that these findings will enable the design of smart bio-inspired materials with responsive and tailored function via a balance of hydrogen bonding character, structural organization, and mechanics.

Introduction

Shape memory polymers (SMPs) are an expanding class of stimuli-responsive materials driven by increasing demands for lighter weight systems with multi-functional and tunable properties for diverse application fields such as biotechnology, textiles, aerospace and electronic devices.[1–5] SMPs are capable of memorizing a permanent shape, fixing a temporary shape, and recovering the permanent shape again in response to an external trigger, such as heat, solvent (water), light, electricity, magnetic field or pH.[6] For a polymer to display the shape memory effect (SME), two structural features are necessary: 1) a fixed phase or cross-linking network, also called a net-point, which dictates the permanent shape of a polymer, and 2) a reversible or switching phase, which controls molecular mobility and allows for temporary shape fixity and recovery[7–9] Controlling both the extent of shape fixity and recovery as well as the response time of the shape memory response are important considerations when designing SMPs for different

applications.[3,10] For example, SMPs for neural electrodes require slow shape recovery at body temperature, which can be controlled by molecular design of the reversible phase.[10,11] As such, fundamental understanding of the relationship between molecular and architectural features and the shape memory behaviour is vital to tailor shape memory properties and to develop new SMPs.

Segmented polyurethanes have gained prominence as SMPs due to their tunable, microphase-separated structure that arises from incompatibilities between the often flexible soft segment (SS) and strongly hydrogen-bonded (H-bonded) hard segment (HS).[12–14] The physically cross-linked and often crystalline HS acts as a net-point, which governs structural integrity and elasticity, while the SS serves as the switching phase. Heat is the most common shape memory trigger for polyurethanes.[15,16] For thermo-responsive polyurethanes, switching is typically activated via the glass transition temperature (T_g) in an amorphous SS or the melting point (T_m) in a semi-crystalline SS.[17] Previous studies have elucidated the relationship between morphology and shape memory properties of polyurethanes.[18–24] Employing polyurethanes with different HS contents, Ji et al. explored the impact of phase-separated microstructure on shape recovery.[20] As the HS content increased from 40% to 50%, shape recovery decreased dramatically from 90% to 75% due to a shift from an isolated to interconnected architecture. However, the majority of investigations of shape memory polyurethanes primarily focus on the manipulation of thermomechanical behaviour by

[a] Department of Materials Science and Engineering, University of Delaware, 127 The Green, 201 Dupont Hall, Newark, DE. USA. 19716.
[b] Department of Chemical and Biomolecular Engineering, University of Delaware 151 Academy St. Newark, DE, 19716.
‡ These authors contributed equally to this work
* Corresponding author. Email: lkorley@udel.edu

varying SS and HS structure without consideration of the interrelated phase separation and SS ordering on the SME.[15,25,26]

Alternatively, the incorporation of self-assembly motifs into conventional polymers is a promising approach toward tuning or improving the SME as well as thermomechanical properties and morphology.[27] Peptides have received significant research interest as functional building blocks for self-assembly because their thermal and mechanical properties can be tailored through peptidic ordering and hierarchical organization, which are dictated primarily by their secondary structure.[28–32] Peptide-containing polymers are an emerging class of SMPs.[2,33–36] Inspired by the idea that β-sheet crystals are responsible for supercontraction in spider silks, H. Huang et al. utilized peptide blocks as the physically crosslinked net-point of a thermo-responsive biopolymer.[33] Specifically, a block copolymer consisting of semicrystalline poly(ε-caprolactone) (PCL) and β-sheet poly(alanine) (PA) blocks was designed. The semicrystalline PCL blocks served as the switching points, whereas β-sheets of the PA segments acted as the net-points, which led to an increased shape recovery ratio (~97%) compared with conventional PCL-type copolymers. This research suggests that peptide secondary structure can serve as architectural motif to influence shape memory response. To develop highly stretchable polypeptide materials with shape memory response, L. Gu et al. utilized poly(γ-benzyl-L-glutamate)-b-poly(propylene glycol)-b-poly(γ-benzyl-L-glutamate) triblock copolymers (PBLG-b-PPG-b-PBLG) as the SS in poly(tetramethylene ether glycol)-based polyurethanes.[34] These peptide-polyurethane/ureas showed high extensibility (>1600%) and high shape recovery ratio (85-95%). The Young's modulus and shape recovery ratio also increased with increasing peptide content or the relative ratio of α-helix to β-sheet due to the "pseudo" HS character of the peptide blocks. Although these investigations highlight the influence of peptidic ordering on shape memory behaviour, fundamental understanding of the relationship between secondary structure, morphology, and stimuli-responsive shape memory behaviour is still relatively unexplored.

Herein, we examine the importance of peptide secondary structure (e.g. α-helices and β-sheets), SS ordering, and hierarchical organization on thermo-responsive SM properties by utilizing peptide-containing PU systems. To assess the potential of peptides as a handle to tailor SME via hierarchical ordering, we build upon our previous material platform, which demonstrated that the incorporation of peptide motifs, such as poly (β-benzyl-L-aspartate) and poly (ε-carbobenzyloxy-L-lysine), can be utilized to modulate thermal and mechanical properties via hierarchical organization and tunable architectural arrangement.[30] Specifically, we utilize ABA triblocks, where A refers to the peptide segment and B is a synthetic polymer core. Furthermore, these ABA triblocks are incorporated as the SS of non-chain extended polyureas. The secondary structure conformation is tailored by peptide repeat length and content, offering a unique handle for controlling hierarchical organization and response behaviour through strategic network design.[30,37] In-depth understanding of the

relationship between hierarchical architecture and the SME will contribute to developing and expanding smart materials despite limited material choices.

Experimental

Materials and methods

Tetrahydrofuran (THF, Optima grade) and anhydrous N,N-dimethylacetamide (DMAc) were purchased from Fisher Scientific. THF was purified using a solvent purification system (Vacuum Atmosphere Company). Anhydrous DMAc was used as-received. β-Benzyl-L-aspartate (BLA), triphosgene, 1,6-hexamethylene diisocyanate (HDI), and dibutyltin dilaurate (DBTDL), α,ω-Bis(3-aminopropyl)poly(dimethylsiloxane) (PDMS, 2500 g/mol) were purchased from Sigma-Aldrich. PDMS was dried at 95 °C under vacuum for 18 hours prior to use to remove any residual water. BLA N-carboxyanhydride (NCA) was synthesized via established literature procedures.[38,39]

Synthesis of poly(β-benzyl-L-aspartate)-b-poly(dimethylsiloxane)-b-poly(β-benzyl-L-aspartate) (PBLA-b-PDMS-b-PBLA)

PBLA-b-PDMS-b-PBLA was prepared via ring-opening polymerization of BLA-NCA using PDMS as the initiator.[30,37] The polymerization was conducted in a nitrogen atmosphere glovebox. The mole ratio of BLA-NCA:PDMS was altered to yield an average of 5 or 20 repeat units for the PBLA blocks. The solubility of the products varied depending on PBLA repeat length.[30,37] While THF was used for the synthesis of PBLA$_5$-b-PDMS-b-PBLA$_5$, a 60:40 mixture of THF: DMAc was chosen for the synthesis of PBLA$_{20}$-b-PDMS-b-PBLA$_{20}$.

For the synthesis of PBLA$_5$-b-PDMS-b-PBLA$_5$, BLA-NCA (5 g, 20 mmol) and 50 mL of THF were added in an oven dried 250 mL round bottom flask with a magnetic stirrer and a condenser. A solution of diamine-terminated PDMS (5 g, 2 mmol) predissolved in 50 mL of THF was added into the flask. The mixture was stirred for 24 hours before precipitation into deionized water. The mixture was filtered, washed with methanol, and dried under vacuum until constant weight was obtained (Yield: 75%).

For the synthesis of PBLA$_{20}$-b-PDMS-b-PBLA$_{20}$, BLA-NCA (10 g, 40 mmol) was dissolved in a mixture of THF and DMAc in a volumetric ratio of 3:2 (150 mL), in an oven dried 250 mL round bottom flask equipped with a magnetic stirrer and a condenser. 2 g (0.8 mmol) of PDMS predissolved in 25 mL of THF was added into the BLA-NCA solution. The mixture was stirred for 24 hours before precipitation in deionized water. The precipitate was filtered, washed with methanol, and dried under vacuum until constant weight was obtained (Yield: 70%).

For the peptide triblock, the nomenclature An-S-An is used where A refers to PBLA, S indicates PDMS and n denotes the PBLA block length.

Synthesis of non-chain extended PBLA-based polyurea hybrids

As reported previously[30], non-chain extended PBLA polyureas were synthesized with an excess of PDMS to control the peptide weight fraction in the final material. For all samples, an isocyanate/amine ([NCO]:[NH$_2$]) ratio of 1 was used, and the ratio of An-S-An to PDMS was tuned to achieve the desired PBLA content. The PBLA weight fraction was calculated using the following equation:

$$\text{wt\% (PBLA)} = 100 \times \left(\frac{xM_{PBLA}}{xM_{PBLA} + yM_{PDMS} + zM_{HDI}} \right) \qquad (1)$$

where x, y and z are the molar quantities of the PBLA triblock, PDMS and HDI, respectively, and M_{PBLA}, M_{PDMS} and M_{HDI} are the molecular weights of PBLA, PDMS and HDI, respectively.

All polymerizations were conducted in a nitrogen atmosphere glovebox. As an example, the synthesis of A20-20 is described. HDI (0.39 g, 2.3 mmol) was dissolved in 23 ml of 3:1 THF:DMAc in an oven dried 100 mL round bottom flask equipped with a magnetic stirrer and a condenser. To this solution, A20-S-A20 (2 g, 0.2 mmol), predissolved in 12 mL of 3:1 THF:DMAc with 5 drops of DBTDL, was added dropwise for around 20 minutes. This solution was stirred for 16 hours at 60 °C before adding PDMS (5.3 g, 2.1 mmol) dissolved in 12 mL of 3:1 THF:DMAc. The reaction was allowed to proceed for an additional 24 hours. The reaction mixture was precipitated in deionized water, filtered, and the filtrate was washed with water and methanol.. The purified precipitate was dried under vacuum until constant weight to yield a rubbery solid.

The nomenclature for these materials is as follows: AX-Y, where A refers to PBLA, X is the PBLA block length (5 or 20), and Y is the peptide weight percentage. **Table 1** summarizes the polymer composition, number-average molecular weight, dispersity and PBLA weight fraction of these non-chain extended PBLA polyureas.

Film preparation

All films were prepared by solvent casting and subsequently solvent annealing (**Figure S1**). Specifically, PBLA-polyurea and control polyurea films were solvent cast from a 10 wt% THF solution into Teflon molds and allowed to air dry for 24 hrs. The films were then solvent-annealed with a 2:1 THF:DMAc mixture at room temperature for 3 days, and then vacuum dried for 24 hours. Film thicknesses were on the order of 0.25 mm. The mixture of THF and DMAc was used to promote α-helical structures in peptidic-polyurea hybrids derived from A20-S-A20.[29]

Molecular weight characterization

The block length of PBLA in the triblocks were calculated via ^{1}H nuclear magnetic resonance (^{1}H-NMR) (Bruker 600 MHz, CDCl$_3$) spectroscopy using end-group analysis (**Figure S2**). The molecular weights and molecular weight distributions of the PBLA-polyureas were determined relative to polystyrene standards using a TOSOH Bioscience GPC equipped with refractive index and variable wavelength detectors (**Figure S3**). THF was used as the eluent, and the temperature was maintained at 40 °C.

Attenuated total reflection - Fourier transform infrared spectroscopy (ATR-FTIR)

The secondary structures of the triblocks (as-precipitated) and PBLA-polyurea hybrids (solvent-annealed) were characterized using a Thermo Nicolet NEXUS 470 FTIR equipped with a diamond crystal for ATR measurements. Gaussian functions were used to fit the FTIR data in the region from $1680 - 1600$ cm^{-1}. The second derivative was utilized to identify peaks associated with peptide secondary structure (*i.e.* α-helix and β-sheet), and the relative amounts of α-helix and β-sheet content was obtained via calculation of the area under each peak. [40–42]

Atomic force microscopy (AFM)

AFM was conducted on a Bruker Multimode in tapping mode using Bruker antimony doped silicon tips (320 kHz, 125 μm). 1 μm x 1 μm images were collected with 256 scans per line at a frequency of 1 Hz. All images of solvent-annealed films were processed using the Bruker Nanoscope Analysis 1.5 software.

Small-angle X-ray scattering (SAXS)

SAXS data was collected using a Xenocs Xeuss 2.0. X-rays were generated at 50 kV/0.6 mA at a beam wavelength of 1.542 Å (Cu Kα radiation) and a sample-to-detector distance of 1200 mm. The scattered beam was recorded on a CCD detector with a pixel resolution of 172×172 μm. The scattering patterns of solvent-annealed films were recorded over 15 minutes of exposure time at room temperature. Using Foxtrot 3.4.9., 2D patterns were azimuthally integrated to obtain the scattering intensity as a function of scattering vector, q, where $q = 4\pi\sin(\theta)/\lambda$ and 2θ is the scattering angle. Origin 9.6. was utilized for data processing.

Differential scanning calorimetry (DSC)

DSC experiments were performed on a TA instruments Discovery series. Solvent-annealed films were tested at a heating rate of 5 °C/min from -80 to 100 °C under N$_2$ atmosphere. The T$_g$ of PBLA in the first cycle was used to determine transition temperatures for the shape memory experiments.

Tensile testing

Tensile testing was carried out using a Zwick/Roell mechanical testing instrument equipped with a 100 N load cell. Solvent-annealed films were cut into approximately 15×3 mm. All samples were elongated to failure at around 70 °C under a constant strain rate of 100% of the initial gauge length per minute. The modulus was determined using the 1% secant method due to the non-linearity of the tensile curves. At least 3 samples were tested, and testing results are summarized in **Figure S4**.

Dynamic mechanical analysis (DMA)

Solvent-annealed films were examined for the shape memory investigations. DMA studies were performed on a TA Instruments Q800 DMA operating at temperature range of -10 °C to 70 °C at a heating rate of 5 °C/min under N_2 atmosphere. For shape memory experiments, a controlled-strain mode was utilized. In the *first step*, the film was heated from room temperature to 70 °C. The strain was increased at a speed of 100%/min to maintain 10% of the elongated length during the *second step*. During the *third step*, at a constant strain, the temperature was reduced to -10 °C and maintained for 10 min followed by a release of the external force or stress in the *fourth step*. During *the fifth step*, the film underwent shape recovery via heating to 70 °C for 30 min.

Shape fixing refers to the ability of a material to retain a temporary shape by cooling below a transition temperature.[15] The shape fixing behaviour can be quantified via the shape fixing ratio (R_f), which is defined as the ratio of the strain after unloading and the strain at the shape fixing temperature (-10 °C under loading (**Equation 2;** *fourth step*). Shape recovery is achieved by heating the material without any stress (unconstrained) to a temperature higher than the transition temperature. The shape recovery can be quantified via the shape recovery ratio (R_r), which is defined as the ratio between the recovered strain and the fixed strain under stress at the deformation temperature (70 °C) (**Equation 3**; *fifth step*).[8,16]

$$R_f = \frac{\varepsilon}{\varepsilon_{load}} \times 100 \qquad (2)$$

$$R_r = \frac{\varepsilon - \varepsilon_{rec}}{\varepsilon - \varepsilon_i} \times 100 \qquad (3)$$

Where ε_{load}, ε, ε_{rec}, and ε_i represents the maximum strain under load, fixed strain after cooling and unloading, strain after recovery, and initial strain at 70 °C, respectively.

Results and discussion

We examine the influence of hydrogen bonding (H-bonding) arrangements on the thermally-induced shape memory response of linear peptidic polyureas (PPUs). Specifically, PBLA was introduced into the soft domain of a non-chain extended HDI-based polyurea as a triblock copolymer with PDMS (**Figure 1**). Non-chain extended polyureas were chosen to probe how secondary structure affects phase mixing and how this microstructural organization influences SM behaviour. PDMS-based polyureas were used as a platform due to the incompatibility between the siloxane and urea components, allowing for the H-bonding interactions between the HS and peptidic segments to be isolated in this study.[43] We varied both PBLA repeat length and content in order to modulate secondary structure, SS ordering, and physical associations between PBLA and the hard phase. The PBLA length was chosen as either 5 or 20 segments per block (A5-S-A5 and A20-S-A20, respectively) to dictate the preference for either β-sheets or a mixture of α-helices and β-sheets in the final polyurea hybrid. **Table 1** details the molecular weight and dispersity of a series of PPUs as a function of PBLA repeat length and weight fraction. We correlate the peptide secondary conformation and H-bonding organization with the microphase-separated morphology and thermo-responsive shape memory behaviour of the PPUs.

Characterization of peptide secondary conformation and hard segment H-bonding arrangement in PPUs

The properties of peptidic materials are highly influenced by their secondary structures.[30] To determine the fraction of β-sheets and α-helices present in all samples, we utilized ATR-FTIR spectroscopy to examine the amide I carbonyl stretch that occurs between 1600-1680 cm^{-1} (**Figure S5**). The relative amounts of β-sheet and α-helix content also are listed in **Table 1.** In peptidic materials, β-sheet formations give rise to a signal between 1620 and 1645 cm^{-1}, while carbonyl stretching peaks indicative of α-helical formations occur between 1650 and 1660 cm^{-1}.[30,44] The A5-based PPUs show an absence of α-helical formations due to the short peptide repeat length. When the PBLA length is increased to 20 repeat units, a mixture of α-helices and β-sheets is obtained. When comparing the A20-based PPUs to the A20-S-A20 triblock copolymer, a reduction in α-helix content is observed across all A20-based PPU samples. This behaviour may be attributed in part to the influence of the HS, where the presence of short
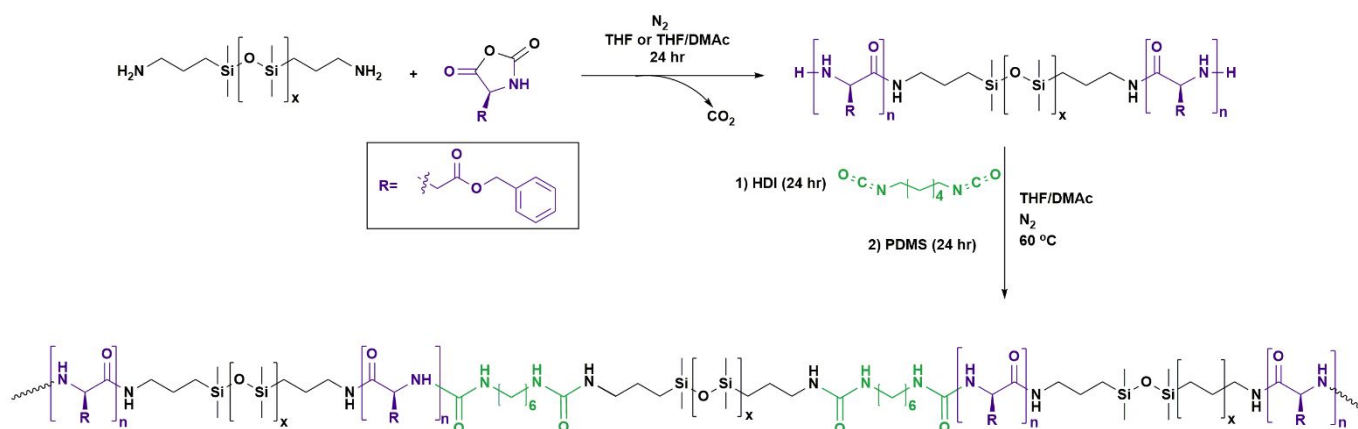
Figure 1. Overall reaction scheme of PPUs

Table 1. Molecular weight, dispersity, and relative amount of peptide secondary structure (β-sheet and α-helix) as a function of PBLA repeat length and content.

	Molecular weight, M_n [a] (kg mol^{-1})	Dispersity, Đ [a]	PBLA[b] (wt%)	α-helix[c] (%)	β-sheet[c] (%)
PDMS-HDI	13.5	1.4	0	-	-
A5-S-A5	-	-	-	0	100
A20-S-A20	-	-	-	43	57
A5-5	14.9	1.5	5	0	100
A5-20	25.5	1.7	20	0	100
A20-5	15.1	1.4	5	18	82
A20-20	15.3	1.5	20	40	60

[a] The dispersity was calculated from GPC using THF as the eluent. [b] Determined from Equation (1). [c] Obtained from the deconvolution of ATR-FTIR absorption bands in amide I stretching region (1600-1680 cm^{-1}).

urea segments drives phase mixing due to intermolecular H-bonding between urea and PBLA segments.[31] This observation will be probed further in examination of the N-H stretch in ATR-FTIR. The α-helix fraction increases from 18% to 40% with increasing peptide content in A20-based PPUs, which can be attributed to the limited mobility in the PPU matrix preventing the formation of intermolecular hydrogen bonds required to form β-sheets and amplifying the intramolecular interactions that drive α-helix formation.

In addition to H-bonding interactions driven by peptide organization, ATR-FTIR can also reveal information about the H-bonding that occurs between the peptide units in the SS and the urea units present in the HS. In segmented polyurethanes, H-bonding within and/or between the SS and HS is the driving force for the development of microphase-separated architectures.[45] In this system, multiple hydrogen bonds can be formed between proton donors (X: urea N-H and amide N-H groups) and proton acceptors (Y: urea C=O, amide C=O, and benzyl ester C=O groups). To examine the impact of PBLA repeat length and content on physical associations between urea linkages and PBLA segments, the N-H stretching absorption region (3200-3450 cm^{-1}) was monitored (**Figure 2A**).[46] 3250-3300 cm^{-1} and 3300-3400 cm^{-1} correspond to symmetrical and asymmetrical stretching, respectively.[47] The

absorption band at 3320-3340 cm^{-1} and ~3450 cm^{-1} is related to H-bonded urea N-H and free N-H, respectively.[43,46,48–50] H-bonded amide N-H stretching appears at 3270-3320 cm^{-1}.[51]

In **Figure 2A**, ATR-FTIR spectra of the control PDMS-HDI polyurea displays a peak with a maximum at 3330 cm^{-1}, indicative of H-bonded urea groups. The addition of 5 wt% of PBLA only slightly impacts the N-H stretching absorption band of both A5-5 and A20-5, implying that HS arrangement is less disrupted by the PBLA segment at the lower peptide loading. Upon incorporation of 20 wt% of PBLA, shifts in the peak position and variations in the peak width are observed. Peak broadening occurs in both A5-20 and A20-20, indicating the presence of differently H-bonded species with a wide range of proton donor-acceptor distances (X-Y distance, where X is urea N-H for this system.)[52]. Peak broadening in segmented polyureas or polyurethanes is also indicative of phase mixing. It was reported that non-chain extended polyurea systems show broader spectra than chain extended polyurea-urethane systems due to phase mixing.[31] However, the band of A5-20 blue-shifts toward higher wavenumber (~3347 cm^{-1}) compared to A5-5, whereas the peak of A20-20 red-shifts toward lower wavenumber (~3317 cm^{-1}) compared to A20-5. In polyurethane systems, the shift in the stretching frequency of the H-bonded groups (e.g. N-H and O-H) is generally a measure
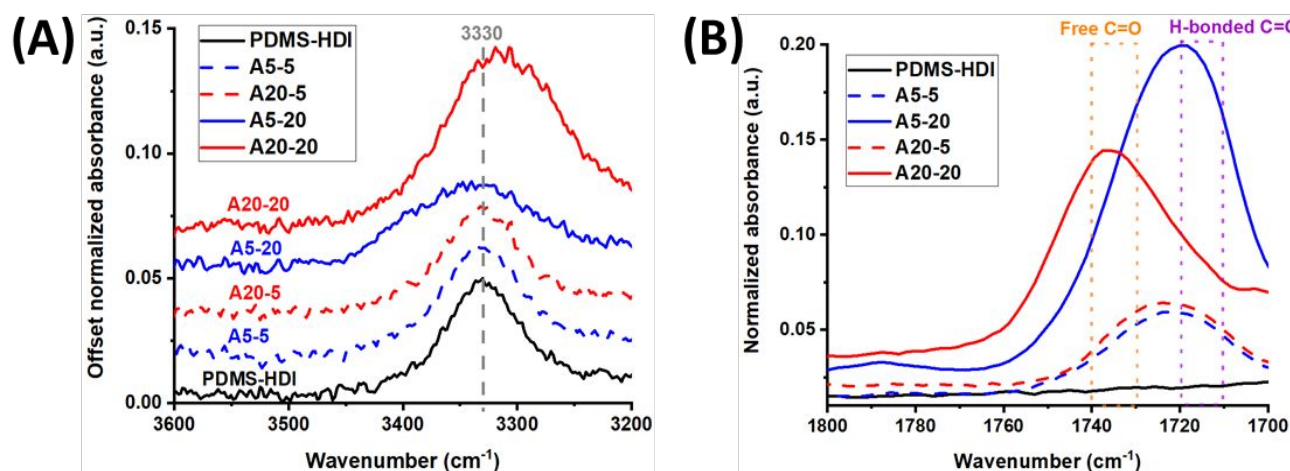
Figure 2. ATR-FTIR investigation of the control PU and PPUs in **(A)** N-H stretching region (3200-3450 cm^{-1}) and **(B)** benzyl ester C=O stretching region (1800-1700 cm^{-1})

of associative strength and X-Y distance in solids.[48,52–54] The shorter X-Y distance and/or stronger H-bonding leads to a shift toward a lower frequency. Thus, while both A5-20 and A20-20 show a broader distribution of hydrogen bond strength due in part of phase mixing, red-shifted A20-20 (β-sheets and α-helices) has more urea groups with stronger H-bonding compared with A5-20 (β-sheets). In other words, A20-20 has more closely-packed and strongly-bonded hard segments, whereas A5-20 possesses less-ordered and weakly-bonded hard segments. This result suggests that secondary structure dictates HS ordering with β-sheets promoting intermolecular H-bonding between peptide and urea segments compared to α-helices which are stabilized by both intramolecular and intermolecular H-bonding and thus less likely to hydrogen bond strongly with urea segments in the HS.

To better understand H-bonding-driven organization in these PBLA-polyurea hybrids, we also examined the C=O stretching absorption bands of the benzyl ester moiety in the PBLA protecting groups (1710-1740 cm^{-1}). The absorption peaks appearing at 1710-1720 cm^{-1} and 1730-1740 cm^{-1} represent the H-bonded C=O groups and free C=O groups of the side chains, respectively.[55,56] **Figure 2B** highlights that the carbonyl peak of A20-20 appears at 1736 cm^{-1}, while the C=O peaks of A5-5, A5-20, and A20-5 emerge at lower wavenumbers (1723-1719 cm^{-1}). These spectroscopic findings

reveal that the C=O groups on the side chain of A20-20 participate less in H-bonding, whereas those of the A5-Y series and A20-5 interact with proton donors in the PBLA segments and/or the hard segments via intermolecular H-bonding. The lack of benzyl ester hydrogen bonds supports the more 'precise' bonding in the HS in A20-20 whereas the opposite is true in the other samples. Thus, this may correlate with peptidic ordering and degree of phase separation.

Figure 3 represents the H-bonding arrangement in PPUs with varying PBLA weight fraction and repeat length. Based on ATR-FTIR results, the variation of peptidic ordering in SS can affect the association between soft and hard blocks, which can also influence hard segmental organization and degree of phase separation. At 5 wt% of PBLA, HS ordering is less disrupted compared to the control (**Figure 2A**) although PBLA-HS interactions exist through urea-amide or/and urea-ester H-bonding (**Figure 2B**). Upon the incorporation of 20 wt% of PBLA, peptidic ordering increases and the secondary structure affects hard segmental arrangement. As the β-sheet content increases (from A5-5 to A5-20), associations between hard segments and β-sheets (PBLA segments) increase via intermolecular H-bonding, which can lead to less ordered hard segments and promote phase mixing. On the other hand, as the relative α-helix content increases (from A20–5 to A20–20), urea-ester H-bonding is absent, supported by **Figure 2B**, and
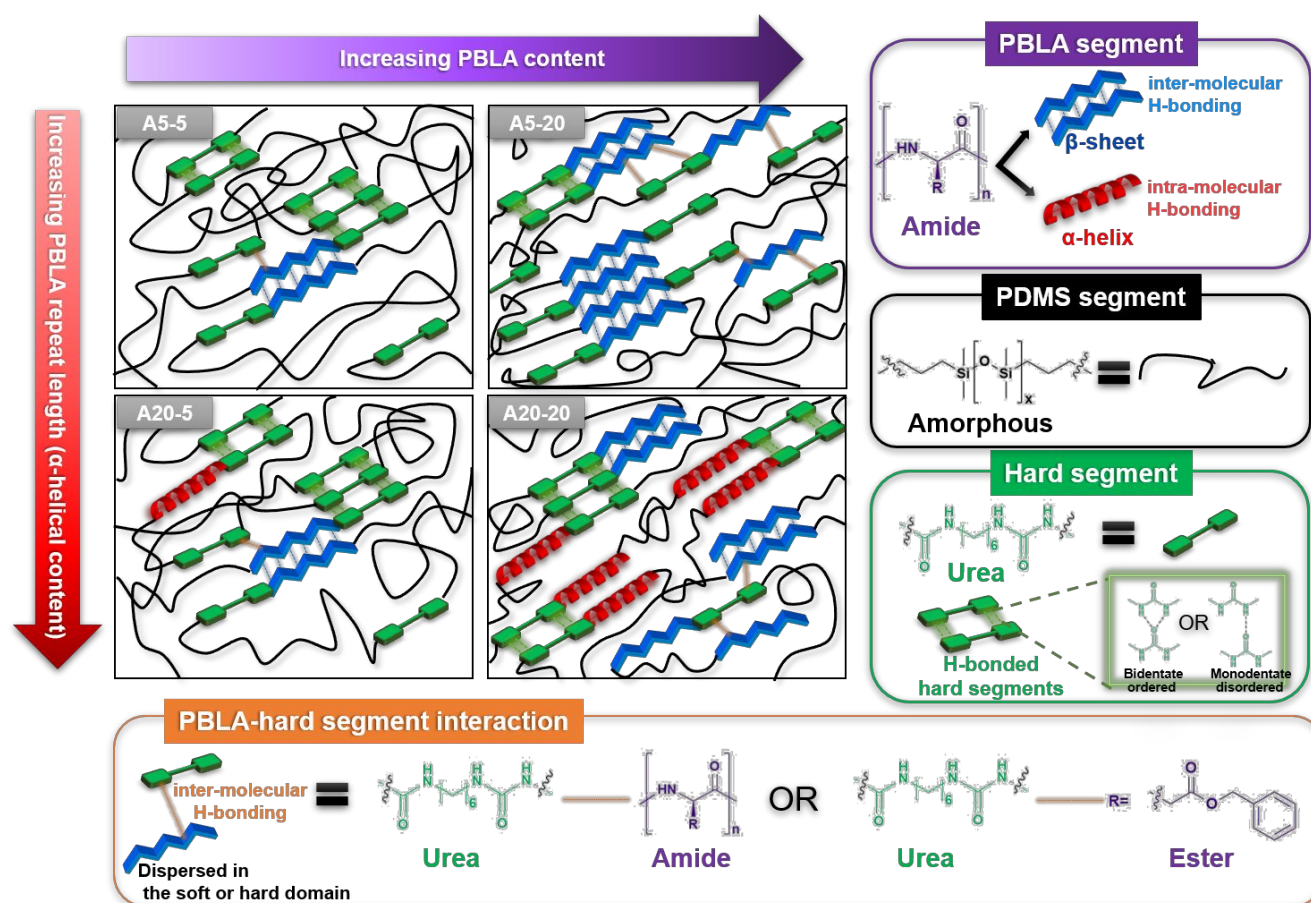
Figure 3. Proposed influence of PBLA content and repeat length on self-assembled H-bonding organization in PBLA-polyurea hybrids (based on ATR-FTIR results). β-sheets are shown as zig-zag planes, and α-helices are denoted as a spiral ribbon. Peptidic ordering influences the arrangement of the hard segments.

mixing between hard and soft segments (PBLA segments) is less favourable compared to A5-20 due to the increased presence of intramolecular hydrogen bonds. We anticipate that variations in the H-bonding arrangement as a function of PBLA secondary structure will modulate the polyurea hybrid microstructure. It is proposed that three morphologies may exist:
1) pure hard domains,
2) pure soft/peptidic domains,
3) mixed phases: hard segments associated with the peptidic domains.

Impact of H-bonding organization on phase separation behaviour and morphology of PPUs

Building upon shifts in secondary structure and associations between the soft and hard phases, the morphology of these PPUs was explored via DSC, SAXS, and AFM investigations. It is expected that the phase behaviour will play a large role in the deformation behaviour of these systems, and, as a result, their shape memory response.

In segmented polyurea and polyurethane systems, DSC is utilized as a method to evaluate phase segregation behaviour by examining variation in thermal transitions of both soft and hard blocks. The PDMS homopolymer typically undergoes a glass transition at -127 °C[30,57,58], which is not included in the temperature range used for these DSC experiments, and two melting transitions (-77 °C and -43 °C)[57]. **In Figure 4A**, the PDMS-HDI control displays two melting regimes associated with the HS at ~44 °C and 85-90 °C as a consequence of different degrees of hard segmental packing despite the absence of chain extension due to both short-

range and longer-range ordering. We attribute this behaviour to the incompatibility in H-bonding between PDMS and HDI; the H-bonding energy of urea-urea and urea-siloxane is 21.8 kJ/mol and 7.5 kJ/mol, respectively.[43] In comparison, a chain extended PDMS-HDI polyurea-urethane exhibited a single melting transition at a higher temperature(~156 °C) due to significant phase segregation.[58]

For PPUs, a PBLA glass transition temperature is additionally observed. At the same PBLA loading, PPUs with a shorter peptide length (A5-5 and A5-20) exhibit a higher T_g compared with those with the longer peptide length (A20-5 and A20-20). As expected, a PBLA loading of 20 wt% also leads to an increase in T_g compared to 5 wt% in both the A5 and A20 series. These findings suggest that the shorter length and increased loading enhance molecular association of the SS, hindering chain mobility. Notably, A5-20 shows a higher PBLA T_g (60.7 °C) than A5-5 and A20-20 by almost three-fold, implying an extensively H-bonded structure.

Figure 4A also indicates that the HS thermal transition is dependent on PBLA content and length, suggesting that peptidic ordering affects hard segmental packing. At the lower PBLA content (5 wt%), the melting transition of the hard domains exists regardless of PBLA length, showing the similar enthalpy of melting for hard phase (ΔH_{HS}) as summarized in **Table S1**. At the higher PBLA content (20 wt%), the HS melting transition of A5-20 completely disappears while that of A20-20 is present at a higher temperature, indicating that A5-20 displays an extensively phase-mixed structure and, as a result, a less ordered HS. It is also important to note that ΔH_{HS} of A20-20 is reduced compared with the control and PPUs with 5 wt%

	q_{max} (Å^{-1})	d_{max} (nm)
PDMS-HDI	0.13	5
A5-5	0.09	7
A5-20	0.07	9
A20-5	0.04	16
A20-20	0.03	21
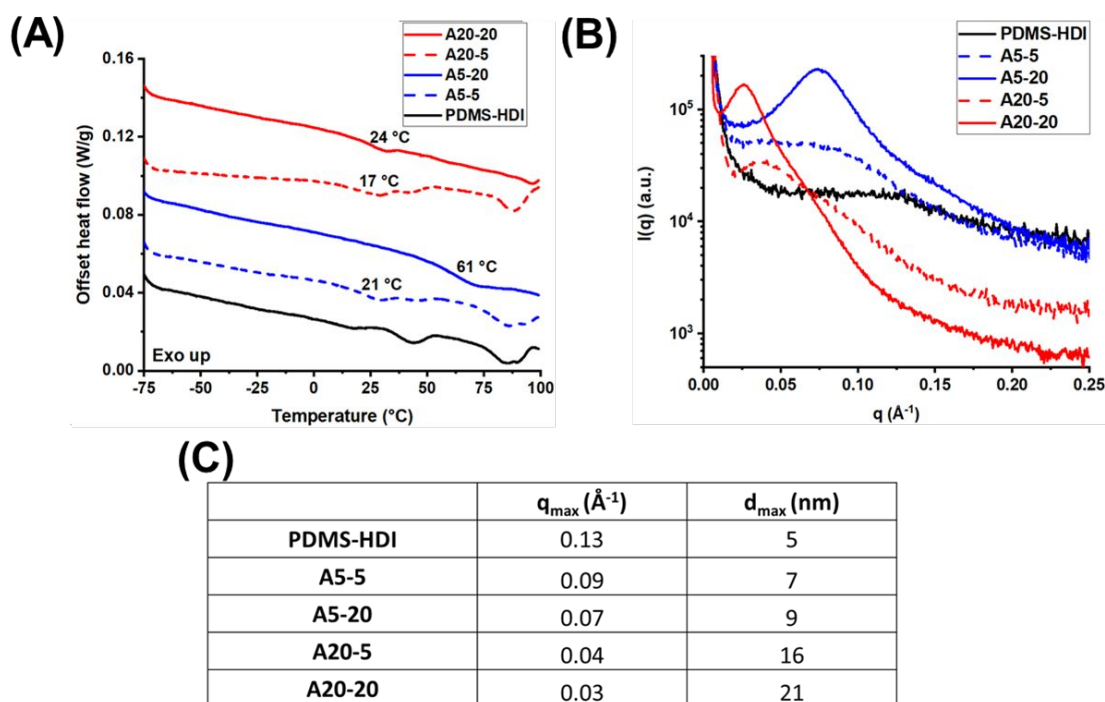
Figure 4. Control PDMS-HDI, A5 and A20 series **(A)** First heating DSC curves of the with the PBLA T_g displayed, **(B)** SAXS patterns at room temperature, and **(C)** Summary of the maxima pseudo hard domain size as a function of PBLA repeat length and weight fraction.
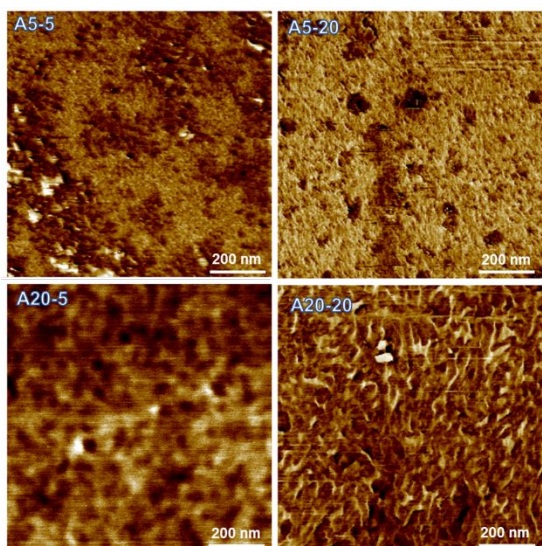
Figure 5. AFM phase images of PPU films

of PBLA, implying that hard segmental packing is disrupted, but the hard phase still remains.

As discussed, the T_g of A5-20 (60.7 °C) is the highest among all samples. Generally, the T_g of the soft domain is also influenced by a degree of phase mixing.[59] Li et. al reported less ordered hard domains resulting in an increase of the SS T_g due to phase mixing.[59] Thus, the dominant β-sheet ordering in the A5 series can disrupt HS packing due to intermolecular H-bonding between the hard and peptide domain, which is supported by ATR-FTIR results. Depression of the melting point as well as the increased PBLA T_g corroborates that intermolecular β-sheet ordering induces phase-mixing compared with intramolecular α-helix ordering.

SAXS is a powerful tool for characterizing nano-scale structures of polymers, such as domain size, inter-domain distance, and the degree of phase separation.[60–62] Typical polyurethanes are considered to contain two distinct phases (crystalline HS and amorphous SS) for the analysis of SAXS data. In our system, the soft phase consists of PBLA-*b*-PDMS-*b*-PBLA triblock copolymers that self-assemble into a fibre-like ordered structure, where the average diameter of the fibres is corresponding to d-spacing obtained from SAXS.[57,63,64] Due to the similar electron density of the PBLA and hard domain and some degree of phase mixing[37,58], discerning the d-spacing of each phase is challenging. As an approach to analysing SAXS data of PPUs, the d-spacing is regarded as a "pseudo" hard domain (peptide+HS) spacing.

As depicted in **Figure 4B**, the control PDMS-HDI exhibits a broad scattering peak with maximum intensity at ~0.13 Å^{-1}, indicating microphase separation with an average hard domain spacing of 5 nm. Upon inclusion of the rigid PBLA segments, all PPUs exhibited a single reflection peak, suggesting the presence of ordered peptidic domains or "pseudo" hard domains. When the PBLA segments are incorporated into the sample, the domain spacing increases, indicating a greater distance between pseudo hard domains. In all cases, increasing the peptide content increases the spacing between the PPU blocks, with domain spacings of 9 nm and 21 nm for

A5-20 and A20-20, respectively, which indicates that the peptide content influences the microphase separation behaviour in PPUs. The disparity in domain spacing between the A5-20 and A20-20 samples is explained by their propensity for phase mixing. As noted in the ATR-FTIR studies, A20-20 exhibits less phase mixing when compared to A5-20 due to the stronger and more well-ordered hydrogen bonds present in its HS. Finally, increasing the PBLA content in the samples decreases the full width at half maximum (FWHM) of the scattering peak, indicating an improvement in the long-range ordering. This behaviour complements the ATR-FTIR data: increasing peptide content increases the number of hydrogen bonds and, as a result, increases ordering of the HS.[37,57,64]

AFM was used to visualize and confirm the phase-segregated morphology probed via SAXS. The phase images (**Figure 5**) reveal fibrillar morphologies that occur across all samples. Beginning with A5-5, short fibres are present in the soft PDMS matrix. This organization is driven both by the alignment of the polyurea HS and the PBLA β-sheet structures perpendicular to the fibre axis.[30] As the PBLA content increases from A5-5 to A5-20, the fibre density also increases while the fibre width is roughly constant. The A20-Y series also display fibrillar structures, where fibres are randomly dispersed in the soft phase. Compared to A20-5, A20-20 forms a densely packed, continuously connected fibre network. Unlike the A5-Y series, the fibre width increases as the PBLA weight fraction increases in the A20-Y series. At the same concentration, the spacing between fibres is higher in A20-20 than A5-20, which is consistent with the SAXS results. These results suggest that the peptide repeat length or secondary structure dictates the fibre width and arrangement of the hard domain. This trend agrees well with our previous work[30] where an increase in fibre width could be explained by the helical axis also lying perpendicular to the fibre axis (maximum helix length ~ 3.2 nm), while the increased size of helical structures drives an increase in fibre width as the peptide content is increased. It is expected that the arrangement of the α-helical structures perpendicular to the fibre axis is heavily influenced by the adjacent hard segments, which have shown propensity to form similar fibrillar bundles in other polyurethane-based systems.[65,66] The role of the morphology in thermomechanical properties and shape memory behaviour will be investigated in the following section.

Shape memory behaviour

In our PPU systems, the ordered PBLA segment serves as the switching phase, and the physically-crosslinked hard phase forms the net-point for shape memory response. The switching temperature for the shape memory experiments was obtained from DSC. The T_g of the PBLA segment in the SS as a function of PBLA repeat length and content is summarized in **Table S1**. The T_g of A5-20 is ~61 °C, which is the highest reported among all PPUs. Accordingly, 70 °C was chosen as the the transition temperature because all PPUs are in the rubbery state at this temperature. It is important to note that two switches are present in the control: the SS T_g and the lower HS
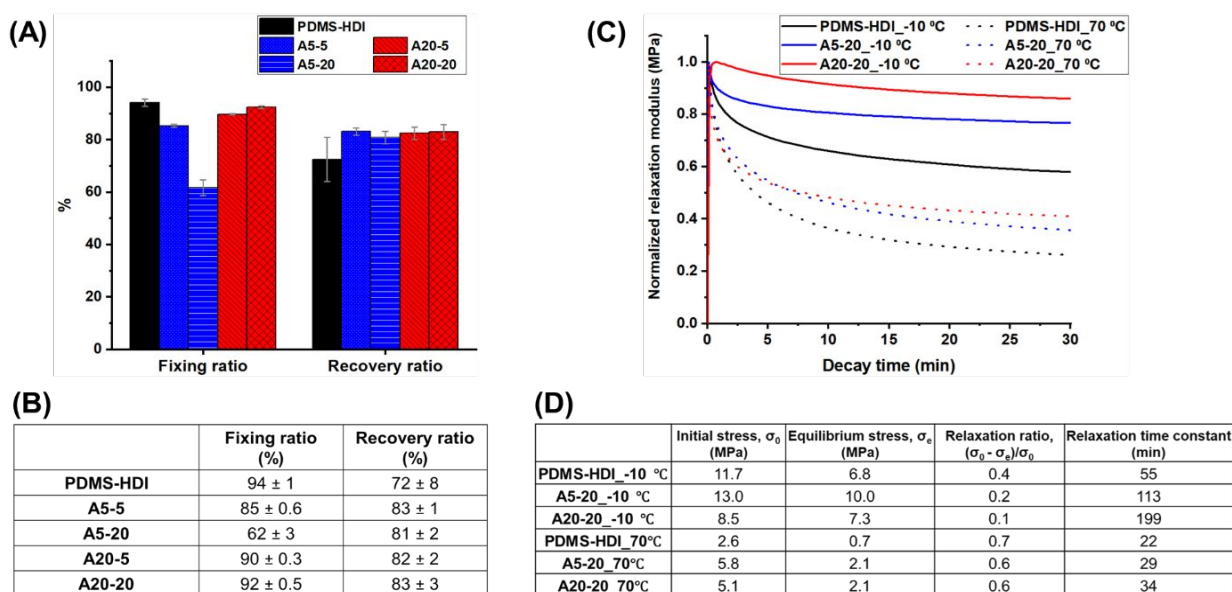
Figure 6. (A) Comparison of shape memory properties; **(B)** Table summarizing shape fixing and recovery ratios of the control and PPUs; **(C)** Stress-relaxation studies for 10% strain at -10 °C and 70 °C. The temperature followed by sample nomenclature indicates the testing value; and **(D)** Table summarizing initial stress, equilibrium stress, relaxation ratio, and relaxation time constant of the control, A5-20 and A20-20.

T_m, which are below 70 °C. Shape memory behaviour was assessed via DMA.

In the shape memory cycle, each PPU was heated to 70 °C to deform the shape and cooled down to -10 °C to fix the shape, followed by heating again to 70 °C to switch from the temporary to the permanent shape. The SME was quantified using Equations 1 and 2. **Figure 6A,B** highlights that the PBLA secondary conformation strongly influences the SM behaviour.

For the A5-Y series, the fixing ratio dramatically decreases from 85% to 62%, and the recovery ratio only slightly decreases from 83% to 81% as the PBLA content increases. In our material system, the peptidic ordering governs shape fixity rather than shape recovery. The reduced shape fixity of A5-20 may be attributed to its morphology. As discussed, A5-20 exhibits less-ordered and weakly-bonded hard segments and displays an extensively phase-mixed morphology due to extensive intermolecular H-bonding with increasing β-sheet content, while A5-5 exhibits distinct two phases. Thus, an increased β-sheet content within the SS disrupts hard segment ordering and reduces the degree of phase separation, leading to a decrease in shape fixity. These findings indicate that a well-separated morphology is critical for good shape fixity.

For the A20-Y series, as the PBLA weight fraction increases, the fixing ratio and recovery ratio remain relatively constant, shifting from 90% to 92%, and from 82% to 83%, respectively. This trend contrasts the A5-Y series. While β-sheet ordering or an increased phase mixing diminishes shape fixity (from 85% to 62%), an α-helical arrangement tends to slightly enhanceshape fixity (90% to 92%). Unlike A5-20, A20-20 exhibits both soft and hard domains, and this phase-separated morphology leads to a higher shape fixing ratio. We further examined the impact of secondary structure by comparing A5-5 and A20-5. The fixing ratio of A20-5 is higher than that of A5-5 although the recovery ratio of both A5-5 and A20-5 remains relatively constant. Based on ATR-FTIR, DSC, SAXS, and AFM

results, it is proposed that, while both exhibit similar microphase segregation behavior, A20-5 contains α-helices and a larger domain spacing and fibre width compared to A5-5, implying that α-helical ordering stabilized by intramolecular H-bonding contributes to improving shape fixity. It is important to note that all PPUs manifest lower shape fixity and higher shape recovery than the control, revealing peptidic ordering enhances chain elasticity and net-point stability. These findings suggest that the peptidic ordering driven by inter- or intra-molecular H-bonding and the degree of phase mixing defines the shape memory response.

To understand the relationship between stress relaxation and shape memory behaviour and to explore the influence of peptidic and hierarchical ordering on viscoelastic properties, stress relaxation studies were conducted at 10% strain at 70 °C (between the PBLA T_g and the HS T_m) and -10 °C (below the PBLA T_g). The stress relaxation in elastomers originates from chain mobility, chain orientation, reorganization of dissociated chains, crosslinks, and entanglements.[67] In all PPUs, the relaxation modulus did not reach zero, which is typically observed in viscoelastic materials (**Figure S6**).[68–70]

Figure 6C highlights the stress relaxation behaviour of PDMS-HDI, A5-20 and A20-20 performed at 10% strain and 70 °C. Compared to the control, both A5-20 and A20-20 have lower relaxation ratio and longer relaxation time. Generally, the remaining stress represents a measure of the driving force for shape recovery. The driving force for shape recovery is the recoiling of polymer chains from a temporary state to a memorized state, also called entropy elasticity.[71,72] Thus, A5-20 and A20-20 exhibit relatively higher recovery ratio, but lower fixing ratio compared with the control due in part to an increase in chain elasticity. This suggests that the incorporation of peptide enhances chain elasticity via the formation of additional physical associations.
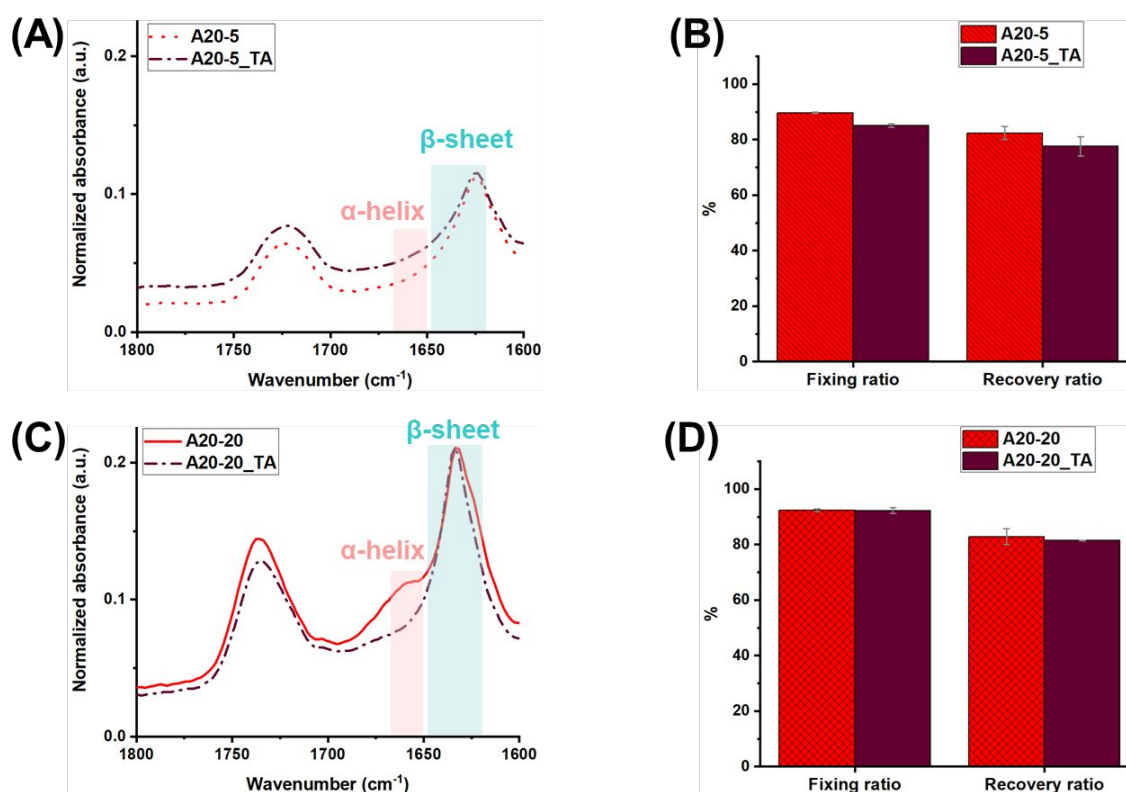
Figure 7. ATR-FTIR spectra and shape memory testing results of A20-5(**(A)** and **(B)**) and A20-20(**(C)** and **(D)**) before and after annealing at 150 °C for 5 minutes. The boxes on the plot highlight stretches associated with α-helices (pink color box) and β-sheets (blue color box), showing the increase in β-sheet content in A20-Y series after annealing.

Figure S6 illustrates the stress relaxation behaviour of the control polyurea and PPUs at -10 °C. At a lower concentration (5%) of PBLA, A5-5 has a lower relaxation ratio than A20-5 due to differences in PBLA arrangement. While both exhibit similar HS packing **(Figure 2 and Figure 4A)** and microphase-separated morphology, A5-5 forms dominantly intermolecular H-bonding and A20-5 contains both intramolecular and intermolecular H-bonding. As the PBLA content increases in both A5-Y and A20-Y series, the relaxation time becomes longer, and the relaxation ratio is diminished. Yet, they exhibit different shape memory properties. While the fixing ratio of A5-20 drastically decreases in comparison to A5-5, A20-20 only slightly increases. We attribute these differences in shape memory response to the degree of phase separation. A5-20 is phase-mixed, whereas A20-20 displays a phase-separated and hierarchical microstructure (**Figure 4**). Based on these experimental findings, we propose that peptidic ordering and extent of phase separation govern viscoelastic and thermo-responsive shape memory properties in these PBLA-based PPUs.

Modulating thermo-responsiveness via PBLA secondary structure tuning

PBLA can undergo a secondary structure transition from α-helix to β-sheet with an increase in temperature. β-sheets are thermodynamically about 260 kJ/mol more stable than α-helices at higher temperature as shown for solid state polyalanine.[29,73] To probe the impact of peptide secondary structure transformation on SM behaviour, the A20-Y series was further investigated. The films were subjected to thermal annealing at 150 °C (above the PBLA T_g and HS T_m) for 5 min to minimize degradation and/or crosslinking.[74] **Figure 7A, C** shows the disappearance of a peak assigned to an α-helix conformation, indicating a reduction in α-helical content as more thermally stable, β-sheets are formed upon cooling.

Shape memory experiments were performed to determine the fixing and recovery ratios of the thermal-annealed A20-Y samples. Upon thermally annealing of A20-5, the shape fixity decreases from 90% to 85%, which agrees with the shape fixity of A5-5 (**Figure 7B**). We assign these changes to newly formed intermolecular β-sheets, which increase chain elasticity. This thermally-induced shape memory behaviour is an excellent example of the influence of secondary structure on tuning the functionality of responsive peptidic polyurea system.

A different picture emerges for A20-20. As shown in **Figure 7D**, the shape fixity ratio of A20-20 is unaffected by the thermal annealing due to the dominate influence of the densely packed and connected fibrous morphology (**Figure 5 and Figure S7**). This observation highlights that the shape memory behaviour is driven by morphology instead of PBLA secondary structure at the higher peptide content. In both A20-5 and A20-20, thermal annealing leads to a decrease in the shape recovery ratio, which is likely due to disruption of the HS packing via thermal annealing.

Conclusions

In this investigation, we utilize non-chain extended polyureas containing PBLA segments in the SS that form either β-sheets

or a mixture of β-sheets and α-helices in order to correlate the effect of secondary structure and hierarchical H-bonding interactions on shape memory behaviour. We demonstrated that the type of SS H-bonding (*i.e.* intermolecular *vs.* intramolecular), the extent of HS packing, and the degree of phase separation, and hierarchical ordering play important roles in determining the shape memory effect. Specifically, peptidic ordering dictates shape memory properties: intra-molecular H-bonding (α-helix dominant) promoted shape fixity, while inter-molecular H-bonding (β-sheet dominant) disrupted shape fixity. However, this scenario is balanced by the impact of a well-separated morphology, which also influences shape memory response. Furthermore, we probed the impact of thermal annealing influenced shape memory behaviour driven by secondary structure changes in the polyurea hybrid. Annealing the A20-Y series at 150 °C shifted the secondary structure from α-helical dominant to primarily β-sheets, leading to a lower shape fixity for A20-5 and constant shape fixity for A20-20. Overall, these investigations highlight that hierarchical morphology and secondary structure play interconnected roles in shape memory behaviour. Changing the nano- and micro-scale interactions of these materials offers convenient avenues for tuning the shape changing capabilities of the film, offering important insight into how self-assembly and multi-level ordering can be used as an avenue for designing stimuli-responsive, bio-inspired materials. This modular material platform can be expanded by incorporating semicrystalline building blocks in lieu of amorphous polymer blocks, adding chain extenders, modifying functional groups on the side chain of the peptide blocks, and utilizing self-assembling components (e.g. peptides) as hard blocks to develop next-generation actuators and sensors for the field of smart textiles, soft robots, and biomaterials.

Conflicts of interest

There are no conflicts to declare.

Acknowledgements

Notes and references

1   J. Hu and S. Chen, *J. Mater. Chem.*, 2010, **20**, 3346–3355.
2   J. Hu, Y. Zhu, H. Huang and J. Lu, *Prog. Polym. Sci.*, 2012, **37**, 1720–1763.
3   L. Gu, Y. Jiang and J. Hu, *Appl. Sci.*, 2017, **7**, 1258–1265.
4   Y. Yang, Y. Wu, C. Li, X. Yang and W. Chen, *Adv. Intell. Syst.*, 2020, **2**, 1900077.
5   B. Zeng, Y. Li, L. Wang, Y. Zheng, J. Shen and S. Guo, *ACS Sustain. Chem. Eng.*, 2020, **8**, 1538–1547.
6   L. Montero De Espinosa, W. Meesorn, D. Moatsou and C. Weder, *Chem. Rev.*, 2017, **117**, 12851–12892.
7   B. K. Kim, J. S. Lee, Y. M. Lee, J. H. Shin and S. H. Park, *J. Macromol. Sci. Part B*, 2001, **40**, 1179–1191.
8   T. Xie, *Polymer*, 2011, **52**, 4985–5000.
9   H. Bhanushali, S. Amrutkar, S. Mestry and S. T. Mhaske, *Shape memory polymer nanocomposite: a review on structure–property relationship*, Springer Berlin Heidelberg, 2021.
10   A. A. Sharp, H. V Panchawagh, A. Ortega, R. Artale, S. Richardson-burns, D. S. Finch, K. Gall, R. L. Mahajan and D. Restrepo, *J. Neural Eng.*, 2006, **3**, L23–L30.
11   H. Gao, J. Li, F. Zhang, Y. Liu and J. Leng, *Mater. Horiz.*, 2019, **6**, 931–944.
12   C. Liu, H. Qin and P. T. Mather, *J. Mater. Chem.*, 2007, **17**, 1543–1558.
13   A. V. Menon, G. Madras and S. Bose, *Polym. Chem.*, 2019, **10**, 4370–4388.
14   Z. Xu, Y. Cui, T. Li, H. Dang, J. Li and F. Cheng, *Macromol. Chem. Phys.*, 2020, **221**, 1–9.
15   W. M. Huang, B. Yang, Y. Zhao and Z. Ding, *J. Mater. Chem.*, 2010, **20**, 3367–3381.
16   A. Shirole, A. Nicharat, C. U. Perotto and C. Weder, *Macromolecules*, 2018, **51**, 1841–1849.
17   S. K. Melly, L. Liu, Y. Liu and J. Leng, *J. Mater. Sci*, 2020, **55**, 10975–11051.
18   J. R. LIN and L. W. CHEN, *J. Appl. Polym. Sci.*, 1998, **69**, 1575–1586.
19   H. M. Jeong, S. Y. Lee and B. K. Kim, *J. Mater. Sci.*, 2000, **35**, 1579–1583.
20   F. L. Ji, J. L. Hu, T. C. Li and Y. W. Wong, *Polymer (Guildf).*, 2007, **48**, 5133–5145.
21   S. Chen, J. Hu, H. Zhuo and S. Chen, *J. Mater. Sci.*, 2011, **46**, 5294–5304.
22   F. L. Ji, J. L. Hu, W. M. W. Yu and S. S. Y. Chiu, *J. Macromol. Sci. Part B Phys.*, 2011, **50**, 2290–2306.
23   W. Xu, R. Zhang, W. Liu, J. Zhu, X. Dong, H. Guo and G. H. Hu, *Macromolecules*, 2016, **49**, 5931–5944.
24   Q. Luo, J. Chen, P. Gnanasekar, X. Ma, D. Qin, H. Na, J. Zhu and N. Yan, *New J. Chem.*, 2020, **44**, 658–662.
25   D. Ratna and J. Karger-Kocsis, *J. Mater. Sci.*, 2008, **43**, 254–269.
26   A. Biswas, V. K. Aswal, B. Ray and P. Maiti, *J. Phys. Chem. C*, 2018, **122**, 11167–11176.
27   C. B. Thompson and L. T. J. Korley, *Bioconjugate Chem.*, 2017, **28**, 1325–1339.
28   O. Rathore and D. Y. Sogah, *J. Am. Chem. Soc.*, 2001, **123**, 5231–5239.
29   S. Tanaka, A. Ogura, T. Kaneko, Y. Murata and M. Akashi,

Macromolecules, 2004, **37**, 1370–1377.

30 J. C. Johnson, N. D. Wanasekara and L. T. J. Korley, *J. Mater. Chem. B*, 2014, **2**, 2554–2561.

31 L. E. Matolyak, J. K. Keum, K. M. Van De Voorde and L. T. J. Korley, *Org. Biomol. Chem.*, 2017, **15**, 7607–7617.

32 L. E. Matolyak, C. B. Thompson, B. Li, J. K. Keum, J. E. Cowen, R. S. Tomazin and L. T. J. Korley, *Biomacromolecules*, 2018, **19**, 3445–3455.

33 H. Huang, J. Hu and Y. Zhu, *Macromol. Biosci.*, 2013, **13**, 161–166.

34 L. Gu, Y. Jiang and J. Hu, *Polymers*, 2018, **10**, 637–648.

35 L. Gu, Y. Jiang and J. Hu, *Mater. Today Commun.*, 2018, **17**, 419–426.

36 P. K. Gavel, D. Dev, H. S. Parmar, S. Bhasin and A. K. Das, *ACS Appl. Mater. Interfaces*, 2018, **10**, 10729–10740.

37 L. Matolyak, J. Keum and L. T. J. Korley, *Biomacromolecules*, 2016, **17**, 3931–3939.

38 R. Katakai and Y. Iizuka, *J. Org. Chem.*, 1985, **50**, 715–716.

39 H. Collet, C. Bied, L. Mion, J. Taillades and A. Commeyras, *Tetrahedron Lett.*, 1996, **37**, 9043–9046.

40 J. K. Kaupplnen, D. J. Moffatt, H. H. Mantsch and D. G. Cameron, *Anal. Chem.*, 1981, **53**, 1454–1457.

41 W. K. Surewicz and H. H. Mantsch, *Biochim. Biophys. Acta - Protein Struct. Mol.*, 1988, **952**, 115–130.

42 A. Dong, P. Huang and W. S. Caughey, *Biochemistry*, 1990, **29**, 3303–3308.

43 E. Yilgör, E. Burgaz, E. Yurtsever and I. Yilgör, *Polymer*, 2000, **41**, 849–857.

44 W. K. Surewicz, H. H. Mantsch and D. Chapman, *Biochemistry*, 1993, **32**, 389–394.

45 C. Tan, T. Tirri and C.-E. Wilen, *Polymers*, 2017, **9**, 184.

46 A. Pangon, G. P. Dillon and J. Runt, *Polymer*, 2014, **55**, 1837–1844.

47 N. Iqbal, M. Tripathi, S. Parthasarathy, D. Kumar and P. K. Roy, *ChemistrySelect*, 2018, **3**, 1976–1982.

48 Y. He, D. Xie and X. Zhang, *J. Mater. Sci.*, 2014, **49**, 7339–7352.

49 N. A. Sears, G. Pena-Galea, S. N. Cereceres and E. Cosgriff-Hernandez, *J. Tissue Eng.*, 2016, **7**, 1–9.

50 X. Chen, C. E. Zawaski, G. A. Spiering, B. Liu, C. M. Orsino, R. B. Moore, C. B. Williams and T. E. Long, *ACS Appl. Mater. Interfaces*, 2020, **12**, 32006–32016.

51 F. S. Parker, in *Applications of Infrared Spectroscopy in Biochemistry, Biology, and Medicine*, Springer US, 1971, 165–172.

52 C. M. Brunette, S. L. Hsu and W. J. MacKnight, *Macromolecules*, 1982, **15**, 71–77.

53 G. C. PIMENTEL and C. H. SEDERHOLM, *J. Chem. Phys.*, 1956, **24**, 639–641.

54 S. L. Hsu, J. Patel and W. Zhao, in *Molecular Characterization of Polymers*, eds. M. I. Malik, J. Mays and M. R. B. T.-M. C. of P. Shah, Elsevier, 2021, pp. 369–407.

55 S.-W. Kuo and C.-J. Chen, *Macromolecules*, 2011, **44**, 7315–7326.

56 Y. S. Lu and S. W. Kuo, *RSC Adv.*, 2015, **5**, 88539–88547.

57 E. Ibarboure, E. Papon and J. Rodríguez-Hernández, *Polymer*, 2007, **48**, 3717–3725.

58 J. C. Johnson, N. D. Wanasekara and L. T. J. Korley, *Biomacromolecules*, 2012, **13**, 1279–1286.

59 T. Li, T. Zheng, J. Han, Z. Liu, Z. X. Guo, Z. Zhuang, J. Xu and B. H. Guo, *Polymers*, 2019, **11**, 838–855.

60 M. Song, H. S. Xia, K. J. Yao and D. J. Hourston, *Eur. Polym. J.*, 2005, **41**, 259–266.

61 S. Pongkitwitoon, R. Hernández, J. Weksler, A. Padsalgikar, T. Choi and J. Runt, *Polymer*, 2009, **50**, 6305–6311.

62 Q. Tian, I. Krakovský, G. Yan, L. Bai, J. Liu, G. Sun, L. Rosta, B. Chen and L. Almásy, *Polymers*, 2016, **8**, 197.

63 P. Papadopoulos, G. Floudas, I. Mate and Ä. P. Fe, *Biomacromolecules*, 2006, **7**, 618–626.

64 E. Ibarboure, J. Rodríguez-Hernández and E. Papon, *J. Polym. Sci. Part A Polym. Chem.*, 2006, **44**, 4668–4679.

65 L. T. J. Korley, B. D. Pate, E. L. Thomas and P. T. Hammond, *Polymer*, 2006, **47**, 3073–3082.

66 J. P. Sheth, D. B. Klinedinst, G. L. Wilkes, I. Yilgor and E. Yilgor, *Polymer*, 2005, **46**, 7317–7322.

67 H. Xia, S. J. Shaw and M. Song, *Polym. Int.*, 2005, **54**, 1392–1400.

68 J. Ivens, M. Urbanus and C. De Smet, *Express Polym. Lett.*, 2011, **5**, 254–261.

69 A. Tcharkhtchi, S. Abdallah-Elhirtsi, K. Ebrahimi, J. Fitoussi, M. Shirinbayan and S. Farzaneh, *Polymers*, 2014, **6**, 1144–1163.

70 X. Li, Q. Hou, J. Zhang, Q. Cui, S. Xu and X. Ding, *Polym. Eng. Sci.*, 2021, **61**, 1624–1637.

71 J. Xu and J. Song, *Proc. Natl. Acad. Sci. U. S. A.*, 2010, **107**, 7652–7657.

72 S. Farzaneh, J. Fitoussi, A. Lucas, M. Bocquet and A. Tcharkhtchi, *J. Appl. Polym. Sci.*, 2013, **128**, 3240–3249.

73 K. A. Henzler Wildman, D. K. Lee and A. Ramamoorthy, *Biopolymers*, 2002, **64**, 246–254.

74 K. Zhang, A. M. Nelson, S. J. Talley, M. Chen, E. Margaretta, A. G. Hudson, R. B. Moore and T. E. Long, *Green Chem.*, 2016, **18**, 4667–4681.